

## **Journal of Thermal Stresses**



ISSN: 0149-5739 (Print) 1521-074X (Online) Journal homepage: https://www.tandfonline.com/loi/uths20

# Thermal deflection and thermal stresses in a thin circular plate under an axisymmetric heat source

### A. H. Elsheikh, Jiajie Guo & Kok-Meng Lee

To cite this article: A. H. Elsheikh, Jiajie Guo & Kok-Meng Lee (2018): Thermal deflection and thermal stresses in a thin circular plate under an axisymmetric heat source, Journal of Thermal Stresses, DOI: 10.1080/01495739.2018.1482807

To link to this article: <a href="https://doi.org/10.1080/01495739.2018.1482807">https://doi.org/10.1080/01495739.2018.1482807</a>

	Published online: 25 Oct 2018.
Ø.	Submit your article to this journal 🗗
Line	
	Article views: 58





# Thermal deflection and thermal stresses in a thin circular plate under an axisymmetric heat source

A. H. Elsheikh<sup>a,b</sup>, Jiajie Guo<sup>a</sup>, **(i)** and Kok-Meng Lee<sup>a,c</sup>

<sup>a</sup>The State Key Laboratory of Digital Manufacturing Equipment and Technology, School of Mechanical Science and Engineering, Huazhong University of Science and Technology, Wuhan, Hubei, China; <sup>b</sup>Department of Production Engineering and Mechanical Design, Tanta University, Tanta, Egypt; <sup>c</sup>George W. Woodruff School of Mechanical Engineering, Georgia Institute of Technology, Atlanta, Georgia, USA

#### **ABSTRACT**

Motivated by the need to investigate thermal effects on the deflection and stresses in a thin-wall workpiece during machining, the thermal problem is modeled with an axisymmetric input to emulate the heat generated at the tool-workpiece interface in a turning process. Using a compressor disk as an illustrative example, the boundary value problem is formulated with a plate model where the perimetric edge is clamped and insulated, and the upper and lower surfaces are subjected to heat convection. The closed form solution of temperature distribution is obtained via Green's function method, based on which the thermal deflection/stresses are obtained in serial forms from the plate constitutive relations. The obtained solutions have been numerically verified with finite-element analysis (FEA), where simulations have been performed for three different materials with discrepant thermomechanical properties to study the thermal effects on the induced deflection and stresses. The analytical result is justified by its good agreement with FEA and its time efficiency in computation offers advantages in potential real-time application to manufacturing process monitoring.

#### **ARTICLE HISTORY**

Received 12 March 2018 Accepted 28 May 2018

#### **KEYWORDS**

Green's function; heat conduction; thermal deflection; thermal stresses; thin-wall plate

#### Introduction

Thin-wall components, featured with low weight and high strength, have been widely employed in aeronautic and aerospace applications in which extreme service demands require for hard-to-machine materials. However, their low thermal conductivities often result in concentrated heating during machining. The non-uniform dynamic heating coupled with the small flexural rigidity gives rise to complicated deflections and stress distributions. As residual deformations and stresses would seriously compromise final product qualities, an in-depth understanding of thermal behavior of a thin-wall component under various types of loadings and boundary constraints is of great practical and theoretical importance [1–6]. As an illustrative example of thin-wall components, this article investigates thermal deflection and thermal stresses induced in a disk-like workpiece under turning processes, where the workpiece is modeled as a thin circular plate clamped at its outer edge and subjected to an axisymmetric heat source due to machining.

The quality of machined workpieces is seriously influenced by the cutting heat, which is featured with high amplitudes and high gradients especially for those materials with low thermal

CONTACT Jiajie Guo Siajie.guo@hust.edu.cn The State Key Laboratory of Digital Manufacturing Equipment and Technology, School of Mechanical Science and Engineering, Huazhong University of Science and Technology, Wuhan, Hubei, 430074, China.

conductivities. This generated heat results in undesirable high temperature gradients, thermal deflections, and thermal stresses, which may impair the mechanical and metallurgical properties [7], as well as induce residual stresses [8] and deformation [9] in workpieces. Therefore, thermally induced stresses must be taken into consideration during design and manufacturing processes of thin-wall components. This may be achieved by carrying out thermal analysis to determine the temperature distribution across the workpiece followed by stress analysis based on the calculated temperatures distribution as well as any mechanical loads or constraints imposed on the workpiece.

Cases of thermal deflections [10-14], thermal stresses [15,16], or both of them [17-19] have been investigated on thin circular plates of solid [10-14,17-19] and annular [15,16] shapes under different inputs and boundary constraints as summarized in Table 1. In most cases, the Dirichlet condition is assumed to prescribe temperatures for the upper surfaces [10,11,13,17,19], lower surfaces [11-14,17,19], and perimetric surfaces [11,13,16,18], which is the simplest to implement in the mathematical formulation. However, it is an ideal case in practice as it requires a complicated control scheme to maintain the constant temperature in a dynamic environment; and hence, it is not suitable for industrial applications such as the machining case under-investigation. Prescribed heat fluxes on the boundaries are mathematically modeled as the Neumann boundary condition. Insulated (heat flux = 0) [10,12,14-19] and nonhomogeneous (heat flux  $\neq$  0) [10,12,17] versions of the Neumann boundary condition have been considered. Finally, the convection boundary condition has been applied on different plate surfaces [6,15,16]. Analyses involving integral transforms [10-14,17,18], Bessel's functions [19], and Homotopy [16] have been carried out and numerical techniques such as the finite difference method [15] have been developed for different applications. Most studies on the thermoelastic problem of thin-wall plates are analytical in nature [10-14,16-18]. This is due to the fact that analytical solutions reveal the effect of different parameters and material thermomechanical properties on the thermoelastic behaviors of thin-wall plates, despite the more simplifying assumptions used in obtaining the analytical closed-form solutions compared with numerical solutions. Moreover, most of these studies considered the plane stress

Table 1. Summary of the previous research works on the thermal stresses of thin circular plates.

Reference	B	oundary conditi		Results			
	Upper	Lower	Perimetric	Internal	Method	Deflection	Stress
[10]	T=0	Insulation	Time-varying <i>q</i>	/	Integral transforms	V	×
[11]	T=0	T=0	Time-varying T	/	Integral transforms	$\sqrt{}$	×
[12]	Insulation	T=0	Time-varying <i>q</i>	Heat generation	Integral transforms	$\checkmark$	×
[13]	Constant T	Constant T	Constant T	Heat generation	Integral transforms	$\sqrt{}$	×
[14]	Ramp- type heating	T=0	Insulation	/	Integral transforms	$\sqrt{}$	×
[15]	Convection	Convection	Insulation; moving uniform <i>q</i>	/	Finite differ- ence method (FLUENT)	×	$\sqrt{}$
[16]	Convection	Convection	Constant <i>T</i> ; Insulation	/	Homotopy analysis	×	$\sqrt{}$
[17]	Convection Prescribed <i>T</i>	Convection $T = 0$	Prescribed <i>q</i> Insulation	/	Integral transforms	$\checkmark$	$\sqrt{}$
[18]	Insulation	Insulation	T=0	Heat generation	Integral transforms	$\sqrt{}$	$\sqrt{}$
[19]	Prescribed T	T=0	Insulation	,	Bessel's functions	$\sqrt{}$	$\sqrt{}$
Current work	Convection	Convection	Insulation	Axisymmetric heat source	Green's function	$\sqrt{}$	$\sqrt{}$

T: temperature; q: heat flux.

state rather than the plane strain state as the later showed inappropriate results when compared with experimental observations [20].

To emulate machining conditions in practice, the convection boundary condition is assumed in the current study for both upper and lower surfaces of the plate with its outer edge fixed by a lathe chuck and subjected to an axisymmetric heat source at the cutting region. The analytical method of the Green's function is employed with the technique of variable separation [21] to determine the temperature. Thermal deflection and stresses are also obtained based on the calculated temperature considering the state of plane stresses. The obtained results provide a basis for analyzing thermal displacement and stresses in a workpiece for manufacturing applications where delicate sensing techniques, such as laser, strain-gauges or infrared imaging, are limited under the complicated machining condition. Furthermore, the obtained results are compared with finite element analysis with COMSOL Multiphysics under the same conditions [22,23]. The remainder of this article offers the following:

- The governing time-dependent heat conduction with the thermoelastic equation of the thin circular plate under study is formulated as a boundary value problem.
- The Green's function method is used to solve the time-dependent heat conduction problem.
- The variable separation technique is used to derive the Green's function for the problem in hand under the prescribed BCs.
- Based on the derived temperature distribution, the closed-form solutions of the thermal deflection and thermal stresses in a thin circular plate are obtained.
- Results have been numerically verified with simulated FEA for three different materials with discrepant thermomechanical properties to figure out the effects of these properties on the induced thermal deflection and stresses.

#### **Problem formulation**

As shown in Figure 1, a thin-wall workpiece under lathe-machining is modeled as a circular plate (of radius a and thickness h) whose coordinates are described with  $0 \le r \le a$ ,  $0 \le \theta \le 2\pi$ , -h/ $2 \le z \le h/2$  in the cylindrical coordinate at the center. As the workpiece is rotated with the outeredge clamp at  $\Omega$  and machined by the tool moving along the horizontal radius, the heat generated at the tool-workpiece interface can be modeled as an axisymmetric input at  $(r_c, z_c = h/2)$ . It is assumed that the upper and lower surfaces  $(z = \pm h/2)$  of the plate are subjected to heat convection while the perimetric surface (r = a) is thermally insulated. As the workpiece is properly fixed in manufacturing applications, it is assumed that the deflection is dominant by the out-of-plane displacement w along the z-axis, and linear thermoelastic constitutive relations are employed in the following formulation.

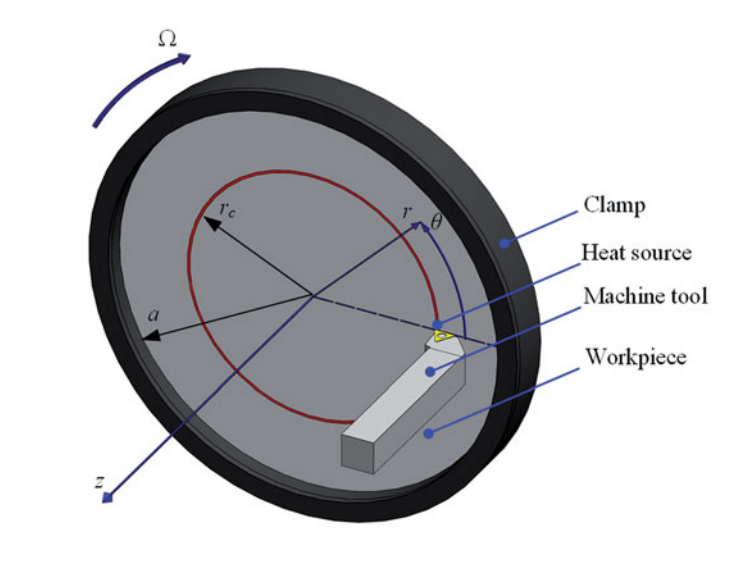
The thermal deflection of an isotropic thin-wall plate is characterized by the displacement field w(t, t)r, z), the Goodier's thermoelastic potential displacement function  $\zeta(t,r,z)$  and the temperature distribution T(t, r, z) via the following governing equations derived from references [21,24,25].

$$\nabla^2 T + \frac{g}{k_t} = \frac{1}{\alpha} \frac{\partial T}{\partial t} \tag{1}$$

$$D\nabla^4 w = -\frac{\nabla^2 M_T}{(1-v)} \tag{2}$$

$$\nabla^2 \zeta = (1 + v)\alpha_t \Delta T \tag{3}$$

where  $k_t$  is the thermal conductivity, the thermal diffusivity is defined as  $\alpha = k_t/\rho c$  with  $\rho$  and cdenoting the density and specific heat, respectively.  $g(t, r, z) = g_1(t)\overline{\delta}(r-r_c)\overline{\delta}(z-z_c)$  represents an axisymmetric heat source, where  $g_1$  is an instantaneous line heat source, and  $\bar{\delta}$  is a Dirac delta



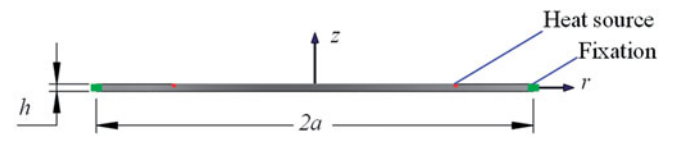


Figure 1. Thin circular plate with an axisymmetric heat source under turning operation.

function that characterizes the location of the line heat source at  $r_c$  and  $z_c$ .  $\Delta T (= T - T_0)$  is the temperature deviation from the initial temperature  $T_0$ . The Laplace operator in the cylindrical coordinate is simplified as  $\nabla^2 = \frac{\partial^2}{\partial r^2} + \frac{1}{r} \frac{\partial}{\partial r} + \frac{\partial^2}{\partial z^2}$  since the component  $\frac{\partial^2}{r^2 \partial \theta^2}$  vanishes in the axisymmetric case. D is the flexural rigidity and  $M_T$  is the thermal moment that are given by

$$D = \frac{Eh^3}{12(1-v^2)}, \quad M_T = \alpha_t E \int_{-h/2}^{h/2} \left( T(r,z,t) - T_0 \right) z dz \tag{4}$$

where E, v and  $\alpha_t$  are Young's modulus, Poisson's ratio and thermal expansion coefficient of the plate material, respectively, and  $T_{\infty}$  is the ambient temperature.

The fixed outer edge of the plate is described by

$$w|_{r=a} = \zeta|_{r=a} = 0, \quad \frac{dw}{dr}\Big|_{r=a} = \frac{d\zeta}{dr}\Big|_{r=a} = 0$$
 (5)

and the initial and boundary constraints on the temperature distribution are given as

$$T|_{t=0} = T_0(r, z) (6)$$

$$T|_{r=0} < \infty \tag{7}$$

$$\left. \frac{\partial T}{\partial r} \right|_{r=0} = 0$$
 (8)

$$-k_t \frac{\partial T}{\partial z}\Big|_{z=h/2} = k_c (T|_{z=h/2} - T_{\infty})$$
(9)

$$k_t \frac{\partial T}{\partial z} \bigg|_{z=-h/2} = k_c (T|_{z=-h/2} - T_{\infty})$$
 (10)

where  $k_c$  is the heat transfer coefficient. The stresses  $\sigma_{rr}$  and  $\sigma_{\theta\theta}$  are given by

$$\sigma_{rr} = -2\mu \frac{1}{r} \frac{\partial \zeta}{\partial r}; \quad \sigma_{\theta\theta} = -2\mu \frac{\partial^2 \zeta}{\partial r^2}$$
 (11)

where  $\mu$  is Lamé constant, while the remaining stresses  $\sigma_{zz}$ ,  $\sigma_{rz}$ , and  $\sigma_{\theta z}$  vanish due to the assumed plane-stress state, and  $\sigma_{r\theta}$  is zero due to the axial symmetry of the problem.

#### **Determination of temperature field**

The Green's function method is employed to solve the formulated BVP that is modified with the homogeneous boundary conditions. The temperature field T(t, r, z) is divided into two components,  $T = T_{\infty} + \psi$ , where the constant ambient component  $T_{\infty}$  satisfies Eq. (1) with g(t, r, z) = 0and the dynamic component  $\psi$  satisfies the following equation:

$$\frac{\partial^2 \psi}{\partial r^2} + \frac{1}{r} \frac{\partial \psi}{\partial r} + \frac{\partial^2 \psi}{\partial z^2} + \frac{g}{k_t} = \frac{1}{\alpha} \frac{\partial \psi}{\partial t}$$
 (12)

$$\psi|_{t=0} = T_0 - T_{\infty} \tag{13}$$

$$\psi|_{r=0} < \infty$$
 (14)

$$\left. \frac{\partial \psi}{\partial r} \right|_{r=a} = 0 \tag{15}$$

$$\left( -k_t \frac{\partial \psi}{\partial z} - k_c \psi \right) \Big|_{z = \frac{k}{2}} = 0$$
(16)

$$\left(k_t \frac{\partial \psi}{\partial z} - k_c \psi\right)\Big|_{z = -\frac{h}{2}} = 0$$
(17)

Employing the variable separation technique  $\psi(t,r,z) = \psi_1(t)\psi_2(r)\psi_3(z)$ , the homogeneous form of Eq. (12) with g(t, r, z) = 0 is decoupled into three ordinary differential equations:

$$\frac{d\psi_1}{dt} + \alpha \lambda^2 \psi_1 = 0 \tag{18}$$

$$\frac{d^2\psi_2}{dr^2} + \frac{1}{r}\frac{d\psi_2}{dr} + \delta^2\psi_2 = 0 \tag{19}$$

$$\frac{d^2\psi_3}{dz^2} + \beta^2\psi_3 = 0 {20}$$

where  $\lambda$ ,  $\delta$ , and  $\beta$  are the corresponding eigenvalues and they satisfy  $\delta^2=\lambda^2$  –  $\beta^2$ . The solutions are obtained as:

$$\psi_1(t) = q_1 e^{-\alpha \lambda^2 t} \tag{21}$$

$$\psi_2(r) = q_2 J_0(\delta r) + q_3 Y_0(\delta r)$$
 (22)

$$\psi_3(z) = q_4 \cos(\beta z) + q_5 \sin(\beta z) \tag{23}$$

where  $J_0$  and  $Y_0$  are Bessel's functions of the zeroth order,  $q_i$ 's (i = 1, 2, ..., 5) are coefficients to be determined from the initial and boundary conditions.

The requirement of a finite temperature at the disk center given by Eq. (14) leads to  $q_3 = 0$ ; besides, the boundary condition (15) produces the characteristic equation to determine  $\delta$ :

$$J_1(\delta_i a) = 0 (24)$$

Both Eqs. (16) and (17) determine  $q_4$  and  $q_5$  for different  $\beta$ 's satisfying the following relations:

$$q_4 = 0 \text{ for } \tan\left(\frac{\beta h}{2}\right) = -\frac{k_t \beta}{k_c}$$
 (25)

$$q_5 = 0$$
 for  $\tan\left(\frac{\beta h}{2}\right) = \frac{k_c}{k_t \beta}$  (26)

The general solution to the BVP stated in Eqs. (12)–(17) with g(t, r, z) = 0 is obtained as:

$$\psi(t;r,z) = \sum_{i=1}^{\infty} \sum_{j=0}^{\infty} J_0(\delta_i r) \left( q_{i,2j} e^{-\alpha \lambda_{i,2j}^2 t} C_{\beta_{2j}z} + q_{i,2j+1} e^{-\alpha \lambda_{i,2j+1}^2 t} S_{\beta_{2j+1}z} \right)$$
(27)

where  $C_{\beta_{2j}z}=\cos(\beta_{2j}z)$  and  $S_{\beta_{2j+1}z}=\sin(\beta_{2j+1}z)$  are employed for simplicity;  $\beta_{2j}$ 's and  $\beta_{2j+1}$ 's are determined from Eqs. (26) and (25), respectively,  $\delta_i$ 's are determined from Eq. (24), and  $\lambda_{ij}^2=\delta_i^2+\beta_j^2$  ( $i=1,\,2,\,\ldots,\,j=0,\,1,\,2,\,\ldots$ ). It is noted that q's in Eqs. (21)–(23) are combined into  $q_{i,2j}$ 's and  $q_{i,2j+1}$ 's which are obtained by substituting Eq. (27) into Eq. (13):

$$q_{i,2j} = \frac{1}{\eta_{i,2j}} \int_0^a \int_{-h/2}^{h/2} r' J_0(\delta_i r') C_{\beta_{2j} z'} (T_0(r', z') - T_\infty) dr' dz'$$

$$\frac{1}{\eta_{i,2j}} \int_0^a \int_{-h/2}^{h/2} dz' (S_0 t) S_{0,2j} (T_0(t', z') - T_\infty) dr' dz'$$

$$q_{i,2j+1} = \frac{1}{\eta_{i,2j+1}} \int_0^a \int_{-h/2}^{h/2} r' J_0(\delta_i r') S_{\beta_{2j+1} z'}(T_0(r',z') - T_\infty) dr' dz'$$

where 
$$\eta_{i,0} = \frac{\beta_0 h + S_{\beta_0 h}}{\beta_0} \frac{a^2 J_0^2(\delta_i a)}{4}$$
,  $\eta_{0,0} = \frac{\beta_0 h + S_{\beta_0 h}}{\beta_0} \frac{a^2}{4}$ ,  $\eta_{i,2j} = \eta_{i,2j+1} = \frac{a^2 h J_0^2(\delta_i a)}{4}$ .

From the above, the Green's function is obtained as

$$G(t,r,z;t',r',z') = \sum_{i=1}^{\infty} \sum_{j=0}^{\infty} r' J_0(\delta_i r') J_0(\delta_i r) \left[ \frac{e^{-\alpha \lambda_{i,2j}^2(t-t')}}{\eta_{i,2j}} C_{\beta_{2j}z'} C_{\beta_{2j}z} + \frac{e^{-\alpha \lambda_{i,2j+1}^2(t-t')}}{\eta_{i,2j+1}} S_{\beta_{2j+1}z'} S_{\beta_{2j+1}z} \right]$$
(28)

So, the solution to the boundary value problem defined by Eqs. (1) and (6-10) is

$$T(t,r,z) = T_{\infty} + \int_{0}^{a} \int_{-h/2}^{h/2} G(t,r,z;t',r',z')|_{t'=0} (T_{0}(r',z') - T_{\infty}) dr' dz'$$

$$+ \frac{\alpha}{k_{t}} \int_{0}^{t} \int_{0}^{a} \int_{-h/2}^{h/2} G(t,r,z;t',r',z') g(t',r',z') dr' dz' dt'$$
(29)

For a special case where  $T_0 = T_{\infty}$  and  $g(t, r, z) = 1(t)\delta(r - r_c)\delta(z - z_c)$  with 1(t) denoting a unit step function, the transient temperature field is given as follows

$$T = T_0 + \frac{r_c}{k_t} \sum_{i=1}^{\infty} \sum_{j=0}^{\infty} J_0(\delta_i r_c) J_0(\delta_i r) \left[ \frac{1 - e^{-\alpha \lambda_{i,2j}^2 t}}{\lambda_{i,2j}^2 \eta_{i,2j}} C_{\beta_{2j}z_c} C_{\beta_{2j}z} + \frac{1 - e^{-\alpha \lambda_{i,2j+1}^2 t}}{\lambda_{i,2j+1}^2 \eta_{i,2j+1}} S_{\beta_{2j+1}z_c} S_{\beta_{2j+1}z_c} \right]$$
(30)

#### Distributions of displacement and stresses

Let the solution of Eq. (2) is given in the following form [14]:

$$w(t,r) = \sum_{i=1}^{\infty} C_i(t) \left[ J_0(\delta_i r) - J_0(\delta_i a) \right]$$
(31)

Applying the biharmonic operator to w(r) in Eq. (31) and using the following result [26]:

$$\nabla^2 J_0(\delta_i r) = -\delta_i^2 J_0(\delta_i r) \tag{32}$$

It is obtained that:

$$\nabla^4 w = \sum_{i=1}^{\infty} C_i \delta_i^4 J_0(\delta_i r) \tag{33}$$

The thermal moment could be obtained by substituting Eq. (30) into Eq. (4):

$$M_T = c_M \sum_{i=1}^{\infty} \sum_{j=0}^{\infty} \kappa_{ij} (1 - e^{-\alpha \lambda_{i,2j+1}^2 t}) J_0(\delta_i r)$$
 (34)

where 
$$c_M = \frac{\alpha_t r_c E(hk_c + 2k_t)}{k_t^2}$$
,  $\kappa_{ij} = \frac{J_0(\delta_i r_c) S_{\beta_{2j+1} z_c} S_{\beta_{2j+1} \frac{h}{2}}}{\lambda_{1,2j+1}^2 \beta_{2j+1}^2 \eta_{1,2j+1}} \left( \text{for } z_c = h/2, \ \kappa_{ij} = \frac{J_0(\delta_i r_c)}{\lambda_{1,2j+1}^2 \beta_{2j+1}^2 \eta_{1,2j+1}} \right)$ 

Then,

$$\nabla^2 M_T = -c_M \sum_{i=1}^{\infty} \sum_{j=0}^{\infty} \kappa_{ij} \delta_i^2 (1 - e^{-\alpha \lambda_{i,2j+1}^2 t}) J_0(\delta_i r)$$
 (35)

Substituting Eqs. (35) and (33) into Eq. (2) yields

$$-D(1-v)\sum_{i=1}^{\infty}C_{i}\delta_{i}^{4}J_{0}(\delta_{i}r) = -c_{M}\sum_{i=1}^{\infty}\sum_{j=0}^{\infty}\kappa_{ij}\delta_{i}^{2}(1-e^{-\alpha\lambda_{i,2j+1}^{2}t})J_{0}(\delta_{i}r)$$
(36)

where  $C_i$  is obtained as follows:

$$C_i(t) = \frac{c_M}{D(1-v)} \sum_{i=0}^{\infty} \frac{\kappa_{ij}}{\delta_i^2} (1 - e^{-\alpha \lambda_{i,2j+1}^2 t})$$
 (37)

and the thermal deflection is given as follows:

$$w(t,r) = \frac{c_M}{D(1-v)} \sum_{i=1}^{\infty} \sum_{i=0}^{\infty} \frac{\kappa_{ij}}{\delta_i^2} (1 - e^{-\alpha \lambda_{i,2j+1}^2 t}) \left[ J_0(\delta_i r) - J_0(\delta_i a) \right]$$
(38)

The temperature in Eq. (30) is represented in the following form:

$$\Delta T = \sum_{i=1}^{\infty} F(z, t) J_0(\delta_i r)$$
(39)

where

$$F(z,t) = \frac{r_c}{k_t} \sum_{j=1}^{\infty} J_0(\delta_i r_c) \left[ \frac{1 - e^{-\alpha \lambda_{i,2j}^2 t}}{\lambda_{i,2j}^2 \eta_{i,2j}} C_{\beta_{2j}z_c} C_{\beta_{2j}z} + \frac{1 - e^{-\alpha \lambda_{i,2j+1}^2 t}}{\lambda_{i,2j+1}^2 \eta_{i,2j+1}} S_{\beta_{2j+1}z_c} S_{\beta_{2j+1}z} \right]$$
(40)

Then substituting Eq. (39) into Eq. (3) provides the following:

$$\nabla^2 \zeta = (1 + v)\alpha_t \sum_{i=1}^{\infty} F(z, t) J_0(\delta_i r)$$
(41)

$$\zeta = -(1+v)\alpha_t \sum_{i=1}^{\infty} \frac{F(z,t)}{\delta_i^2} \left( J_0(\delta_i r) - J_0(\delta_i a) \right)$$
(42)

Finally, the stress state in the disk,  $\sigma_{rr}$  and  $\sigma_{\theta\theta}$ , can be obtained by substituting Eq. (42) directly into Eq. (11) as follows:

Table 2. Material properties.

Materials	Density $\rho$ (kg/m <sup>3</sup> )	Conductivity $k_t$ (W/m-K)	Specific heat $C_p$ (J/kg-K)	Diffusivity $\alpha$ (10 <sup>-6</sup> m <sup>2</sup> /s)	Coefficient of linear thermal expansion $\alpha_t$ (10 <sup>-6</sup> 1/K)	Young's modulus E (GPa)	Poisson's ratio $v$
Aluminum	2700	200	900	82.31	23.4	69	0.33
AISI 4340	7850	44.5	475	11.93	12.3	205	0.28
Ti-6Al-4V	4430	6.7	526	2.88	7.06	105	0.33

$$\sigma_{rr} = -2\mu(1+\upsilon)\alpha_t \sum_{i=1}^{\infty} \frac{F(z,t)}{\delta_i r} J_1(\delta_i r)$$

$$\sigma_{\theta\theta} = -2\mu(1+\upsilon)\alpha_t \sum_{i=1}^{\infty} \frac{F(z,t)}{2} \left( J_0(\delta_i r) - J_2(\delta_i r) \right)$$
(43)

#### **Numerical calculations and discussion**

The derived expressions for the temperature, deflection, and stress provide important insights into the role of the thermomechanical material properties in elastic behaviors of the thin circular plates under axisymmetric heating. The temperature distribution in the plate is only dependent on its thermal properties such as thermal diffusivity and thermal conductivity. On the other hand, the plate deflection and stress are dependent on both thermal and mechanical properties, such as thermal diffusivity, thermal conductivity, coefficient of linear thermal expansion, Young's modulus, and Poisson's ratio.

The numerical calculations have been carried out for three different materials (Aluminum 6063-T83, Steel AISI 4340, and Titanium Ti-6Al-4V alloy), which have discrepant mechanical and thermal properties as illustrated in Table 2. It is assumed that the plate is subjected to a constant line heat source of  $g_1 = 200$  W/m with the initial temperature  $T_0(r, z) = 0$ . The heat transfer coefficient between the upper and lower surfaces and their surroundings is also assumed to be constant with  $k_c = 20$  W/m<sup>2</sup> K.

Figure 2 shows the temperature, for the three materials under-investigation, along the disk radius at the upper surface (z = h/2) when the heat source is located at ( $r_c = 120 \,\mathrm{mm}$  and  $z_c = 0.0025 \,\mathrm{mm}$ ) after 3000 s. The obtained results show good agreement with those obtained from COMSOL Multiphysics for the three materials under study. As shown in Figure 2, the titanium disk has the highest temperature gradient as well as the highest peak temperature at the heat source location followed by the steel disk and the aluminum disk. This is due to the very low thermal diffusivity of titanium ( $2.91 \times 10^{-6} \,\mathrm{m}^2/\mathrm{s}$ ) compared with those of steel ( $1.19 \times 10^{-5} \,\mathrm{m}^2/\mathrm{s}$ ) and aluminum ( $8.27 \times 10^{-5} \,\mathrm{m}^2/\mathrm{s}$ ).

Figure 3 shows the temperature for the titanium disk along the disk radius at the lower surface (z = -h/2) when the heat source is located at  $r_c = 120$  mm and  $z_c = 0.0025$  mm at different times ranged from 20 s to 6000 s. The disk temperature increases with the time as shown in Figure 3; however, the increasing rate slows down with the time as it approaches the steady-state.

Figure 4 shows the steady-state temperature (for  $t = 3000 \,\mathrm{s}$ ) along the radius on the lower surface (z = -h/2) of the titanium disk, where the heating source is applied at different  $r_c$ 's on the upper surface (z = h/2). In Figure 4(a), the heat source is specified with a constant intensity of  $g_1 = 200 \,\mathrm{W/m}$ ; as the heating location changes with  $r_c$ , the maximum temperature  $T_{\mathrm{max}}$  stays around 83 °C for  $r_c = 30$ , 60, and 90 mm, and it becomes 95 and 133 °C for  $r_c = 120$  and 140 mm, respectively. It can be explained that as the heat source approaches toward the insulated boundary, the heat tends to be accumulated locally rather than being dissipated in all directions as it

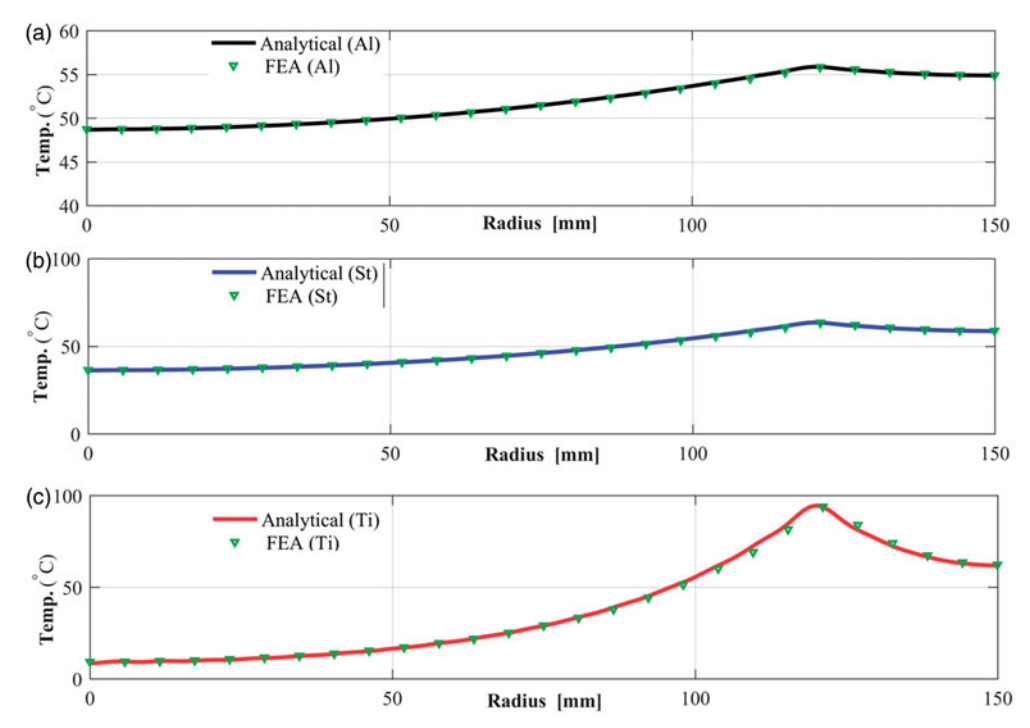


Figure 2. A comparison between the proposed analytical method and COMSOL results for the temperature distribution at the lower surface due to an axisymmetric heat source ( $r_c = 120 \text{ mm}$ ,  $z_c = 0.0025 \text{ mm}$ , and t = 3000 s).

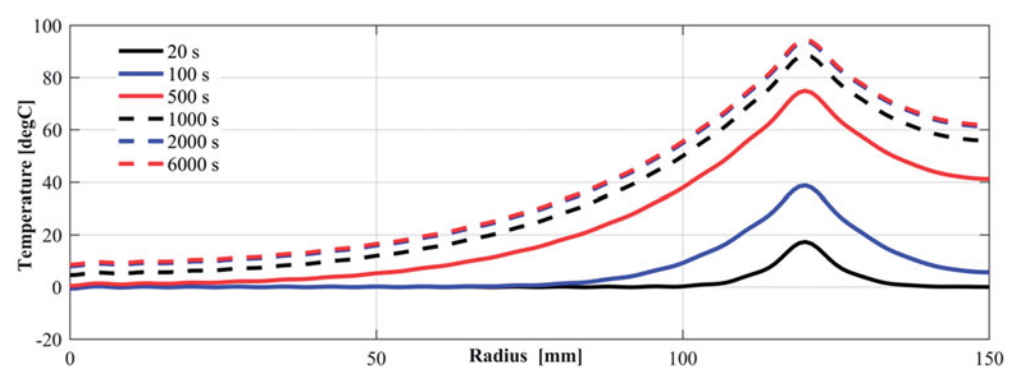
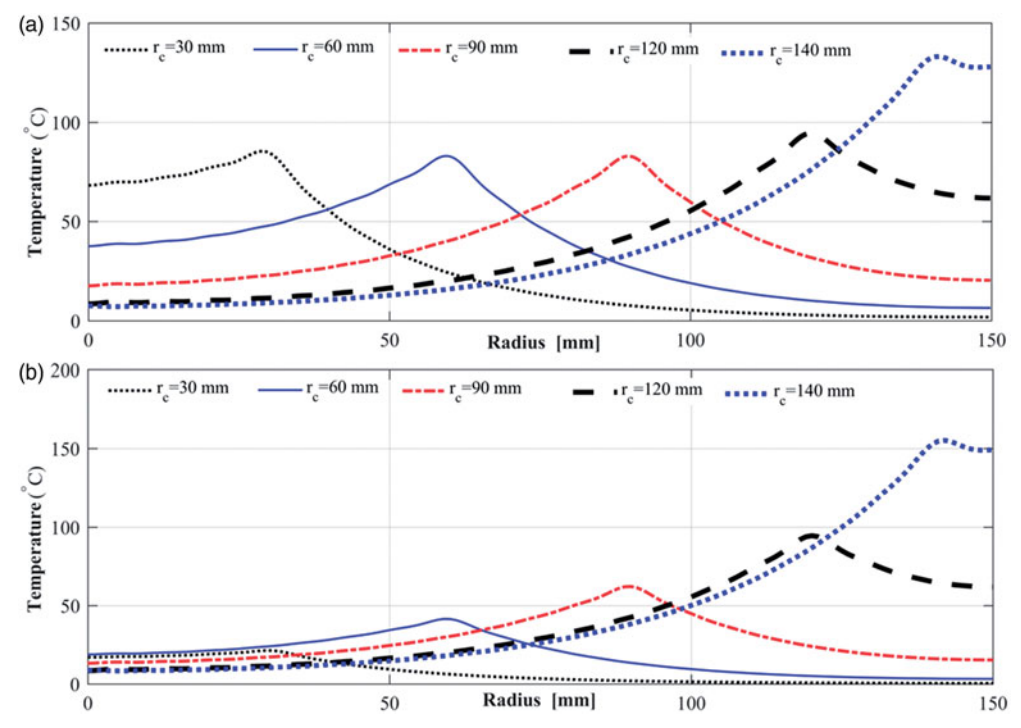


Figure 3. The temperature distribution at the lower surface due to axisymmetric heat source ( $r_c = 120 \, \text{mm}$  and  $z_c = 0.0025 \, \text{mm}$ ) at different times.

does at the median area of the disk. For comparison, the temperature distribution is simulated in Figure 4(b) with the heat source intensity increased proportionally with  $r_c$  that is  $g_1 = 50$ , 100, 150, 200, and 233 W/m for  $r_c = 30$ , 60, 90, 120, and 140 mm, respectively. As shown in Figure 4(b),  $T_{\rm max}$  increases monotonically mainly due to the increased input power with  $r_c$ ; and the rate of change in  $T_{\rm max}$  increases, because less amount of heat is dissipated as the heat source approaches closer to the insulated boundary.

Figure 5 shows the effect of the number of the terms used in summation process according to Eq. (30) on the accuracy of the obtained results. The more terms are included in the summation, the less error is expected. However, less than  $1^{\circ}$ C as a maximum error can be achieved using only 20 terms, where the finite number of terms in the summation results in limited computational



**Figure 4.** The temperature distribution at the lower surface due to axisymmetric heat source ( $z_c = 0.0025 \, \text{mm}$  and  $t = 3000 \, \text{s}$ ) at different radii with (a) constant heat source intensity ( $g_1 = 200 \, \text{W/m}$ ) and (b) increasing heat source intensity with  $r_c$ .

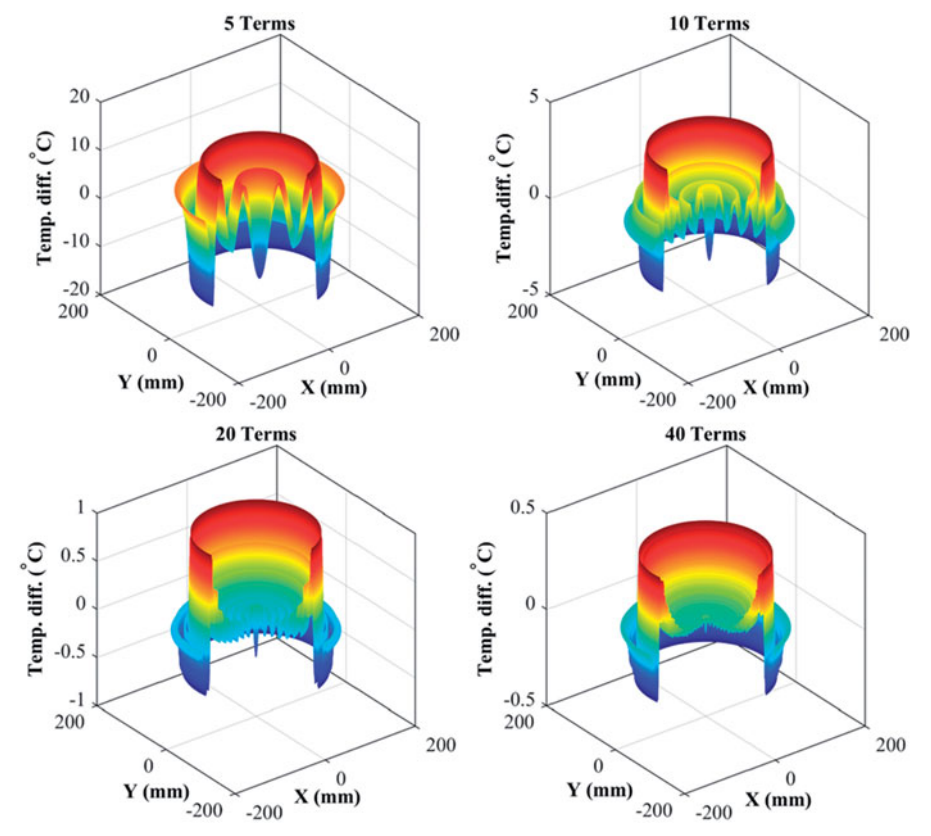


Figure 5. The effect of the number of terms used in summation on the results accuracy.

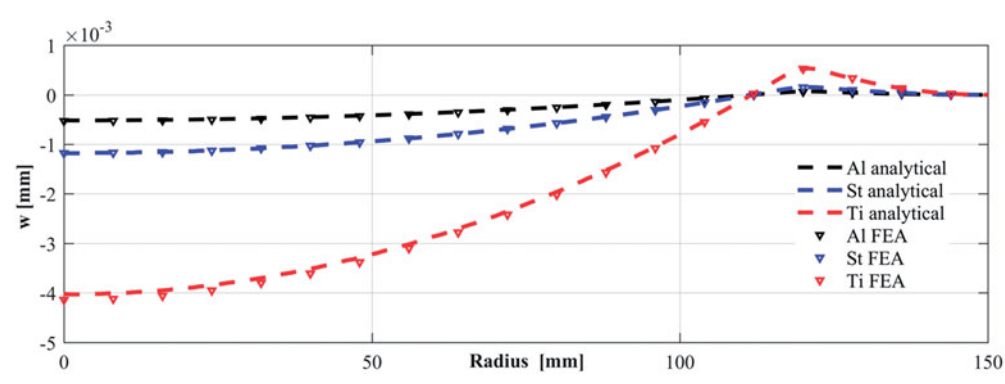


Figure 6. The thermal deflection at the mid-plane due to axisymmetric heat source ( $r_c = 120 \, \mathrm{mm}, \, z_c = 0.0025 \, \mathrm{mm}$ , and

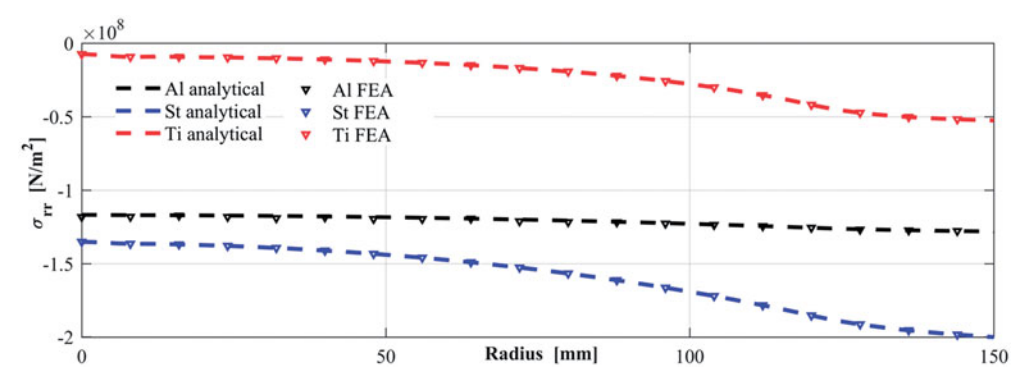


Figure 7. The radial stresses at the upper surface due to axisymmetric heat source ( $r_c = 120 \, \text{mm}$ ,  $z_c = 0.0025 \, \text{mm}$ , and t = 3000 s).

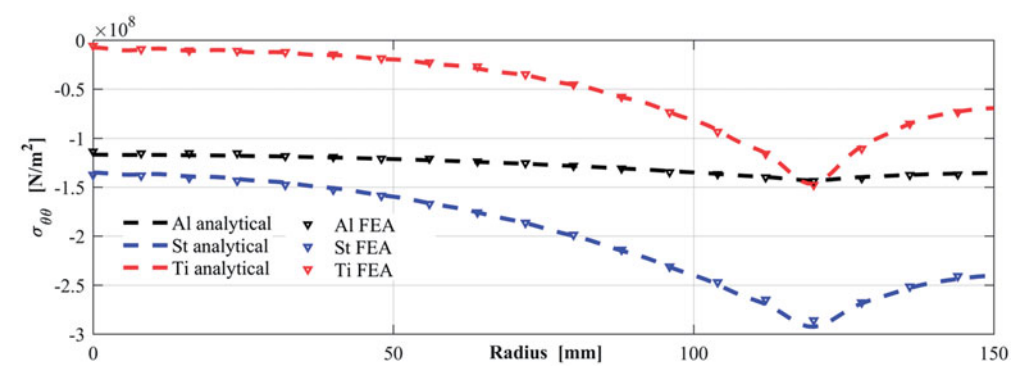


Figure 8. The tangential stresses at the upper surface due to axisymmetric heat source ( $r_c = 120 \, \text{mm}, \, z_c = 0.0025 \, \text{mm}$ , and t = 3000 s).

costs thus makes the proposed method suitable for online monitoring of a machining process. The number of terms used in summation process not only affects the error, but also the smoothness of the results. So, for a certain application the sufficient number of terms can be selected to achieve the target accuracy.

Figure 6 shows the deflection of the mid-plane of the disk (z = 0) for the three materials under the same conditions used to obtain Figure 2. However, the steel and titanium disks have larger Young's moduli (205 and 105 GPa) compared with the aluminum disk (69 GPa), so the steel and titanium disks showed larger deflection than the aluminum disk. It is due to the larger temperature gradients induced in the steel and the titanium disks which results from the lower thermal diffusivity of these materials. This result reveals that the material thermal properties have a dominant effect on the thermal deflection compared to the mechanical properties. Figures 7 and 8 show the radial and the tangential stress components for the three materials under study. The steel alloy has the largest stresses followed by the aluminum alloy and finally the titanium alloy has the smallest stresses. This is due to the smaller modulus of elasticity (105 GPa) and coefficient of linear thermal expansion  $(7.06 \times 10^{-6} \, {\rm K}^{-1})$  of titanium alloy compared with those of steel alloy (205 GPa and  $12.3 \times 10^{-6} \, {\rm K}^{-1}$ , respectively).

#### **Conclusion**

This article investigates the thermal deflection and stresses in a thin-wall circular plate fixed at the outer edge and subjected to an axisymmetric heat source. The upper and lower surfaces are subjected to thermal convection, while the perimetric surface is thermally insulated. First, the mathematical model is constructed, and then the closed-form solutions are determined for the temperature distribution, thermal deflection, and thermal stresses. Numerical calculations have been performed, and the results are illustrated graphically and compared with finite element analysis in COMSOL Multiphysics. The results show that thermal properties have a dominant effect on the thermal deflection of the plate compared to mechanical properties.

#### **Funding**

This research was supported by the National Basic Research Program of China (973 Program, grant no: 2013CB035803), the National Natural Science Foundation of China (grant no: 51505164), and the U.S. National Science Foundation (grant no: CMMI-1662700).

#### **Disclosure statement**

No potential conflict of interest was reported by the authors.

#### **ORCID**

Jiajie Guo (D) http://orcid.org/0000-0002-7740-6792

#### References

- [1] E. Cheung, W. Yuan, and M. Hua, "Physical simulation of the deflection in turning of thin disk-shaped workpieces," *Int. J. Adv. Manufact. Technol.* vol. 15, no. 12, pp. 863–868, 1999. DOI: 10.1007/s001700050143.
- [2] J. Guo, K.-M. Lee, W. Liu, and B. Wang, "Design criteria based on modal analysis for vibration sensing of thin-wall plate machining," *IEEE/ASME Trans. Mechatron.*, vol. 20, no. 3, pp. 1406–1417, 2015. DOI: 10.1109/TMECH.2014.2360371.
- [3] H.-L. Dai, X. Yan, and H.-J. Jiang, "Thermoviscoelastic behavior in a circular HSLA steel plate," *J. Therm. Stress.*, vol. 36, no. 10, pp. 1112–1130, 2013. DOI: 10.1080/01495739.2013.818895.
- [4] M. Yu, J. Guo, and K.-M. Lee, "A modal expansion method for displacement and strain field reconstruction of a thin-wall component during machining," *IEEE/ASME Trans. Mechatron.*, vol. 23, no. 3, pp. 1028–1037, 2018. DOI: 10.1109/TMECH.2018.2790922.



- A. T. Karttunen, R. von Hertzen, J. N. Reddy, and J. Romanoff, "Exact elasticity-based finite element for circular plates," Comput. Struct., vol. 182, pp. 219-226, 2017. DOI: 10.1016/j.compstruc.2016.11.013.
- [6] K.-M. Lee, L. Yang, K. Bai, and J. Ji, "An efficient flexible division algorithm for predicting temperaturefields of mechatronic system with manufacturing applications," IEEE/ASME Trans. Mechatron., vol. 22, no. 4, pp. 1818–1827, 2017. DOI: 10.1109/TMECH.2017.2715559.
- [7] O. Fergani, and S. Y. Liang, "The effect of machining process thermo-mechanical loading on workpiece average grain size," Int. J. Adv. Manufact. Technol., vol. 80, no. 1-4, pp. 21-29, 2015. DOI: 10.1007/s00170-015-6975-8.
- B. Coto, V. G. Navas, O. Gonzalo, A. Aranzabe, and C. Sanz, "Influences of turning parameters in surface [8] residual stresses in AISI 4340 steel," Int. J. Adv. Manufact. Technol., vol. 53, no. 9-12, pp. 911-919, 2011. DOI: 10.1007/s00170-010-2890-1.
- J. Wang, S. Ibaraki, and A. Matsubara, "A cutting sequence optimization algorithm to reduce the workpiece [9] deformation in thin-wall machining," Precis. Eng., vol. 50, pp. 506-514, 2017. DOI: 10.1016/ j.precisioneng.2017.07.006.
- M. N. Gaikwad, and K. C. Deshmukh, "Thermal deflection of an inverse thermoelastic problem in a thin [10] isotropic circular plate," Appl. Mathemat. Model., vol. 29, no. 9, pp. 797-804, 2005. DOI: 10.1016/ j.apm.2004.10.012.
- [11] A. K. Tikhe, and K. C. Deshmukh, "Inverse heat conduction problem in a thin circular plate and its thermal deflection," Appl. Mathemat. Model., vol. 30, no. 6, pp. 554-560, 2006. DOI: 10.1016/j.apm.2005.12.014.
- K. C. Deshmukh, S. D. Warbhe, and V. S. Kulkarni, "Quasi-static thermal deflection of a thin clamped cir-[12] cular plate due to heat generation," J. Therm. Stress., vol. 32, no. 9, pp. 877-886, 2009. DOI: 10.1080/ 01495730903018556.
- K. R. Gaikwad, and K. P. Ghadle, "Nonhomogeneous heat conduction problem and its thermal deflection [13] due to internal heat generation in a thin hollow circular disk," J. Therm. Stress., vol. 35, no. 6, pp. 485-498, 2012. DOI: 10.1080/01495739.2012.671744.
- [14] S. K. R. Choudhuri, "A note on quasi-static thermal deflection of a thin clamped circular plate due to ramp-type heating of a concentric circular region of the upper face," J. Franklin Instit., vol. 296, no. 3, pp. 213-219, 1973. DOI: 10.1016/0016-0032(73)90059-8.
- H. Yapıcı, M. S. Genç, and G. Ozışık, "Transient temperature and thermal stress distributions in a hollow disk subjected to a moving uniform heat source," J. Therm. Stress., vol. 31, no. 5, pp. 476-493, 2008. DOI: 10.1080/01495730801912652.
- M. M. Roozbahani, H. Razzaghi, M. Baghani, M. Baniassadi, and M. Layeghi, "Temperature and stress dis-[16] tribution in hollow annular disk of uniform thickness with quadratic temperature-dependent thermal conductivity," J. Therm. Stress., vol. 40, no. 7, pp. 828-845, 2017. DOI: 10.1080/01495739.2016.1271734.
- K. S. Parihar, and S. S. Patil, "Transient heat conduction and analysis of thermal stresses in thin circular [17] plate," J. Therm. Stress., vol. 34, no. 4, pp. 335-351, 2011. DOI: 10.1080/01495739.2010.550812.
- K. R. Gaikwad, and X.-J. Yang, "Two-dimensional steady-state temperature distribution of a thin circular [18] plate due to uniform internal energy generation," Cogent Mathemat., vol. 3, no. 1, pp. 1135720, 2016.
- V. S. Kulkarni, and K. C. Deshmukh, "Quasi-static thermal stresses in a thick circular plate," Appl. [19] Mathemat. Model., vol. 31, no. 8, pp. 1479-1488, 2007. DOI: 10.1016/j.apm.2006.04.009.
- [20] D. Ball, "Elastic - plastic stress analysis of cold expanded fastener holes," Fatig. Fract. Eng. Mater. Struct., vol. 18, no. 1, pp. 47–63, 1995. DOI: 10.1111/j.1460-2695.1995.tb00141.x.
- [21] D. W. Hahn, and M. N. Ozişik, Heat Conduction, 3rd ed. Hoboken, NJ: John Wiley & Sons, 2012.
- V. Suarez et al., "Study of the heat transfer in solids using infrared photothermal radiometry and simulation by COMSOL multiphysics," Appl. Radiat. Isotopes, vol. 83, pp. 260-263, 2014. 2014/01/01/2014. DOI: 10.1016/j.apradiso.2013.04.010.
- T. Abdelhamid, A. H. Elsheikh, A. Elazab, S. W. Sharshir, E. S. Selima, and D. Jiang, "Simultaneous recon-[23] struction of the time-dependent robin coefficient and heat flux in heat conduction problems," Inverse Problems Sci. Eng., pp. 1-18, 2017. DOI: 10.1080/17415977.2017.1391243.
- [24] J. N. Reddy, Theory and Analysis of Elastic Plates and Shells, 2nd ed. Boca Raton: Taylor & Francis, 2006.
- [25] M. R. Eslami, R. B. Hetnarski, J. Ignaczak, N. Noda, N. Sumi, and Y. Tanigawa, Theory of Elasticity and Thermal Stresses. Netherlands: Springer, 2013.
- [26] B. G. Korenev, Bessel Functions and Their Applications. Boca Raton: CRC Press, 2003.